Fuel 429 (2027) 140829

Contents lists available at ScienceDirect

Fuel

journal homepage: www.elsevier.com/locate/fuel

Full Length Article

Dynamic transient control of hydrogen direct-injection SI engines: effects of ramp duration on engine performance and abnormal combustion

Zayne Zaman [a,*], Mohamed Mohamed [a], Xinyan Wang [a], Hua Zhao [a], Anthony Harrington [b], Jonathan Hall [b]

[a] *Brunel University London, London, United Kingdom*
[b] *MAHLE Powertrain Ltd, Northampton, United Kingdom*

A B S T R A C T

Hydrogen internal combustion engines offer a route to near-zero carbon on-road transport while preserving existing engine manufacturing and calibration know-how. Translating that potential into real-world driving, however, depends on transient control; steady-state maps alone cannot guarantee either safe operation or low NOx emissions during load steps. This paper reports a controlled transient sweep on a 0.4 L single-cylinder direct-injection spark-ignition hydrogen research engine. Five ramp durations (1.38, 1.08, 0.84, 0.48 and 0.24 s) were evaluated at a constant engine speed of 2,000 rpm with a target relative air–fuel ratio of 2.75 under closed-loop feedback control. The measurements track injection pulse width, spark timing, boost, lambda, IMEP, peak in-cylinder pressure and the maximum pressure rise rate (R_{max}) through each transient. As ramp duration is shortened, lambda excursions and air-path overshoot grow rapidly: at 0.24 s the in-cylinder pressure overshoot approaches the mechanical safety limit, IMEP overshoots the steady-state target by about 22 %, and R_{max} exceeds the 600 kPa/°CA calibrated threshold. With a ramp of 0.48 the most hazardous R_{max} peak at roughly 1,000 kPa/°CA is caused, demonstrating that fastest is not always most damaging. Only the 1.38 s baseline keeps all combustion-severity metrics inside their reliability envelope. A feed-forward fuelling term scaled by the rate of manifold pressure change dP/dt is proposed to close the transient lambda gap; with physical implementation and experimental validation proposed as a future optimisation step. The results identify pressure-gradient management as the binding constraint for transient calibration of lean DI hydrogen engines.

1. Introduction

Road transport contributes roughly 20–24 % of global energy-related CO_2 emissions [1]. Despite rapid electrification, more than 90 % of the in-service vehicle fleet still uses an internal combustion engine running on petroleum fuel [2], and regional ICE phase-out plans [3] leave a long transitional decade in which decarbonisation of the existing platform is as important as fleet turnover. Hydrogen spark-ignition engines (H_2-ICEs) are one of the few pathways that use hydrogen without the cost, materials and infrastructure penalties of fuel cells or large batteries [4].

Hydrogen has several properties that make it attractive as an SI fuel: carbon-free at the point of combustion, a high laminar flame speed, and a wide flammability range (4–75 % in air) that allows ultra-lean operation with low NOx when calibrated correctly [5]. Produced by renewable electrolysis, it offers a credible route to lifecycle carbon neutrality [6]. Its disadvantages are equally well known — very low minimum ignition energy and low volumetric energy density, which forces injector nozzle areas typically 3–5 times larger than gasoline for equivalent energy delivery.

While the steady-state combustion, thermal efficiency, and emission characteristics of hydrogen internal combustion engines have been extensively documented, evaluating their operational behaviour under dynamic transient conditions represents a critical frontier for real-world automotive implementation. Transient engine operation introduces severe challenges that do not manifest during steady-state testing. As hydrogen possesses an extremely wide flammability limit and low ignition energy, it is highly sensitive to rapid fluctuations in the local relative air–fuel ratio lambda and in-cylinder residual gas fractions. Recent research has focused heavily on managing these transient transitions; studies exploring the use of variable geometry turbochargers and advanced EGR control loops to mitigate the inherent air-path response lag during sudden transient load transitions [7]. However, existing literature primarily evaluates relatively conservative or heavily compensated transient ramp durations. There remains a critical knowledge gap regarding the fundamental, uncompensated thermodynamic and chemical kinetic boundaries of lean-burn direct-injection hydrogen mixtures when subjected to ultra-fast load sweeps. Investigating these extreme transient acceleration rates is essential for establishing the baseline requirements of next-generation, closed-loop predictive ignition and injection control architectures.

In a hydrogen SI engine, the load can be modulated in two ways.

* Corresponding author.
E-mail address: zayne.zaman@brunel.ac.uk (Z. Zaman).

https://doi.org/10.1016/j.fuel.2026.140829
Received 22 April 2026; Received in revised form 9 July 2026; Accepted 28 July 2026

Nomenclature

Symbol/Abbreviation	Meaning
10 % to 90 % Burn Duration	Crank-angle interval between 10 % and 90 % mass fraction burned
50 % MFB	Combustion Phasing (50 % Mass Fraction Burned)
AFR /λ	Relative Air-Fuel Ratio
aTDCf/aTDCg	After the Top Dead Centre firing/gas exchange
BDI	Barrier Discharge Igniters
BEV	Battery Electric Vehicle
bTDCf/bTDCg	Before the Top Dead Centre firing/gas exchange
BTE	Brake thermal efficiency
BRIC	Band-pass, rectify, integrate, compare (knock detector)
CA 5/10/50/75/90	Combustion phasing location
CAD	Crank Angle Degree
CLD	Chemiluminescent (NOx) detector
CO/CO_2	Carbon Monoxide/Carbon Dioxide
COV_{IMEP}	Coefficient of Variation of IMEP
DAQ	Data Acquisition
DI/PFI	Direct Injection/Port Fuel Injection
ECU/GEC	Electronic Control Unit/ Global Engine Controller
GHG	Greenhouse Gas
H_2/**HC**	Hydrogen/ Hydrocarbons
ICE	Internal Combustion Engine
IMEP	Indicated Mean Effective Pressure
ITE	Indicated Thermal Efficiency
LNV	Lower Net Value
MBT	Minimum spark advance for best torque
NDIR	Non-Dispersive Infrared
NOx/ NH_3	Nitrogen Oxides/Ammonia
K_{ff} /σ_{H2}	Steady-state fuel sensitivity factor / hydrogen transient correction factor
PID	Proportional Integral Derivative
PM	Particulate Matter
PMEP	Pumping Mean Effective Pressure
Rmax	Pressure Rise Rate
SI	Spark Ignition
T_{10} /T_{90}	10 %/90 % Response Time

Quality control adjusts lambda at roughly constant trapped mass, typically by modulating injection pressure or duration. Quantity control adjusts the trapped air mass with throttle or boost and scales fuel to keep lambda constant. In transient operation both control strategies are constrained by a fundamental asymmetry: increasing injection duration to satisfy transient load demands can degrade mixture homogeneity and push lambda away from the target, whereas pneumatic manifold-filling delays in the air path introduce an inherent lag that feedback control loops cannot anticipate. Prior work has shown that transient lean operation with hydrogen is especially prone to cyclic variability and abnormal combustion for exactly this reason [8].

Demonstrations such as the Aston Martin / Alset V12 hydrogen racing programme [9] confirm that boosted hydrogen combustion is viable under extreme loading, but they also illustrate how closely the boost ramp, pulse width and spark must be synchronised during fast transitions. The same concern applies in downsized passenger-car applications, where rapid transient load steps predominate.

Extensive steady-state experimentation has been conducted on hydrogen direct-injection spark-ignition (DI-SI) research engines, including the MAHLE/Brunel University single-cylinder platform utilised in this study. Prior investigations on this architecture have focused on:

- Lean hydrogen combustion stability
- NOx formation mechanisms under ultra-lean conditions
- Pressure rise rate ($dP/d\theta$) characterisation.
- Knock-limited spark advance (KLSA) mapping.
- Boosted hydrogen operation under fixed-speed, fixed-load conditions.

Most of the H_2-ICE literature on the DI platform used here (MAHLE / Brunel single-cylinder research engine) has concentrated on steady-state mapping: lean combustion stability, NOx mechanisms at ultra-lean λ, $dP/d\theta$ characterisation, knock-limited spark advance, and boosted operation at fixed speed and load. Those studies agree that ultra-lean operation ($\lambda > 2.0$) suppresses NOx while preserving indicated efficiency [10–15], that combustion remains stable up to $\lambda \approx 3.0$ with optimised spark timing. Pressure-rise-rate behaviour is strongly coupled to mixture strength and spark timing under boost [16]; aggressive spark advance under lean boosted conditions can lift the pressure gradient and erode knock margin even though hydrogen is commonly treated as knock-resistant [17].

However, most prior experimental campaigns have been conducted for steady state operation at fixed engine speeds and constant load points. Under these conditions, air-path dynamics, injection timing, and ignition control are allowed to reach equilibrium before data acquisition. Consequently, the interaction between boost dynamics, lambda control, and combustion severity during rapid load transients remains insufficiently characterised.

Engines rarely operate in steady-state conditions in reality. Transient load steps, such as rapid throttle transitions, introduce rapid changes in boost pressure, trapped mass, injection duration, and spark phasing. These dynamic interactions can produce lambda excursions, pressure overshoot, and elevated pressure rise rates before closed-loop stabilisation occurs.

Transient hydrogen combustion presents unique risks:

- Rapid fuel lean-to-rich oscillations due to air-path delay
- Boost overshoot leading to elevated in-cylinder peak pressure.
- Amplified pressure rise rates exceeding the engine design limit.
- Increased abnormal combustion likelihood.

The gap between steady-state hydrogen combustion research and transient operation is therefore significant. The challenge lies not in understanding hydrogen combustion fundamentals, but in synchronising rapid control actions (boost, injection PWM, ignition timing, lambda feedback) while maintaining mechanical safety margins.

This study intends to address this research gap by systematically investigating the impact of varying transient intensities. The context being of an on-road light-duty, passenger vehicle application, where downsized engines are increasingly subjected to highly dynamic load changes. This engine platform was used to simulate these conditions defined by ramp duration ranging from 1.38 s to an aggressive 0.24 s. Using a 0.4-litre single cylinder, direct-injection spark-ignition (DI-SI) research engine, this work specifically examined the in-cylinder pressure overshoot ratio and the rate of pressure rise. Testing was conducted under lean-burn conditions at a target lambda of 2.75 to sustain ultra-low NOx emissions. During these fast transients, the inherent delays in air intake, injection, and ignition control could cause lambda excursions, resulting in the air-to-fuel ratio temporarily deviating from the target. The aim of an optimised control is to balance short ramp durations with an acceptable level of transient response deviation.

The area of transient operation is currently still challenging and uncommon to be investigated [18]. Steady-state operation is well studied and there is a wealth of literature available relating to it. This study uses the target lambda as a dynamic variable which will mitigate

NOx peaks by ensuring the air–fuel ratio doesn't remain in a high ***NOx*** region during the ramp. As emphasized in [19] engines face unique transient stability issues due to the high volumetric displacement of gaseous hydrogen and the resulting delays in the intake manifold. These phenomena often lead to rich spikes and increased risk of knock during rapid load steps.

Furthermore, research in Automotive and Engine Technology (2025) demonstrates that positive load ramps often trigger significant ***NOx*** emission peaks during mode switching, necessitated by the decoupling of air and fuel paths. This issue is stabilised with the introduction of a fast response PID loop, providing a robust baseline for multi-cylinder engine management.

The scope of this study is to isolate the fundamental transient response of the lambda control loop; this is the primary limiting factor in combustion stability. This engine acts as a fundamental unit of a multi-cylinder system. There have been examples of such closed-loop PID controllers as being used here whereby calculating the instantaneous error between the Target Lambda and the Actual Lambda. the controller computes a Trimming [20]. Two things transfer directly from the single-cylinder result to a multi-cylinder turbocharged engine: the lambda-to-load step response time, which sets the minimum tolerable ramp for a given Rmax budget, and the per-cylinder lambda-loop logic itself, which acts as the master demand signal for individual injectors regardless of cylinder count. Two things do not transfer: manifold resonance in a multi-cylinder intake, and wastegate dynamics on a turbocharger. A production ECU implementation would need to synchronise the waste-gate controller to the ramp limits found here and would need a global engine controller coordinating across cylinders. The scope of this paper is therefore the algorithmic transferability of the lambda-prioritised control logic, not a production-ready ECU calibration.

The engine specifications are summarised in Table 1.

2. Experimental setup

This section describes the engine, the hydrogen supply system and the data-acquisition chain. As the fuel is hydrogen, the fuel supply is designed around a fail-closed principle: any detectable leak isolates the high-pressure line at the bottle, vents the low-pressure circuit and triggers the cell alarm.

A fast emissions analyser was not available during this campaign; earlier work on the same platform used steady-state analysers. Transient emission measurement is planned for future work (see Section 5).

Table 1
Engine Specifications.

Parameter	Value
Configuration	Single Cylinder
Displaced volume	400 cc
Stroke x Bore	73.9 mm x 83 mm
Compression Ratio	11.3: 1
Number of Valves	4
Exhaust Valve Timing	EMOP (Exhaust Maximum Opening Point) 100–140 CAD BTDC, 11 mm Lift, 278 CAD Duration
Inlet Valve Timing	IMOP (Intake Maximum Opening Point) 80–120 CAD ATDC, 11 mm Lift, 240 CAD Duration
Injection System	Central Direct Injection – Outwardly Opening Spray Nozzle Gasoline Direct Fuel Injection Maximum Fuel Pressure – 20 MPa Hydrogen Direct Fuel Injection Maximum Fuel Pressure – 4 MPa Hydrogen Port Fuel Injection Maximum Fuel Pressure – 1 MPa
Injection Control	MAHLE Flexible ECU (MFE)

2.1. Engine setup

The single-cylinder DI-SI engine carries a dedicated hydrogen injector and is managed by the MAHLE Flexible ECU. The base engine is a gasoline unit converted to run on hydrogen. The H_2 injector can be moved between an intake-port position (PFI 2–10 bar) and a centrally mounted in-cylinder position (DI, up to 40 bar). For this study only the DI configuration was used. An AC dynamometer provides both motoring and braking, and the dyno controller is tied to the throttle-position sensor so that a commanded ramp in throttle translates into a matched dyno load trajectory; engine speed is held at 2,000 rpm throughout.

2.2. Fuel supply system

All hydrogen bottles sit outside the test cell. The hydrogen line enters the cell through two stages of instrumented control panel, each with a pressure sensor, a regulator and a solenoid valve. A programmable logic controller (PLC) monitors the cell: if it detects a hydrogen concentration above 3 % at either the cell-ceiling sensor (which catches buoyant gas) or the engine-hood sensor (which catches crankcase leakage), or if any temperature sensor trips, the PLC closes both solenoid valves, vents the line and signals the emergency shut-down. An ATEX-certified extract fan keeps the cell air changed above the statutory lower limit. As backfire risk is highest with PFI, a 130 °C thermofuse inside the intake manifold provides a mechanical backup even when the PLC path is healthy.

2.3. DAQ system

The DAQ has 138 input channels divided between fast (crank-domain) and slow (time-domain) cards. Combustion events depend on piston position rather than on wall-clock time, so pressure and any derived quantity such as R_{max} are logged in the crank domain to remove timing jitter. The fast channels use an NI USB-6363 and an NI USB-6353; the slow channels, covering exhaust and head temperatures, oil pressure, and the analyser line, run on an NI USB-6210. The three cards are read through a single Vieletech acquisition application. TDC alignment is verified before every run with a motored sweep on the crank encoder.

The cycle of variation (COV_{IMEP}) quantifies the fluctuation in torque and emissions results from one cycle to another. The indicated mean effective pressure of the COV_{IMEP} is calculated using the mean indicated mean effective pressure (IMEP), as shown in Equation (1).

$$COV\_IMEP = (\sigma\_IMEP/IMEP\_mean) \times 100\% \quad (1)$$

Knock detection (*Knock Compare*) shown in Eq. (2) was achieved through the BRIC (Bandpass, Rectify, Integrate, and Compare) method, which accurately detects engine knock occurrence. Background interference was mitigated via a second-order Butterworth IIR bandpass filter, with cutoff frequencies tuned to the specific acoustic resonance of the 0.4 L cylinder geometry. Integration windows were established to isolate the combustion-induced oscillations from valve-train noise. Finally, a threshold-based classification system was implemented to convert the integrated signal into a binary knock/non-knock determination.

$$Knock\ Compare = K\ /\ R;\ knock\ event\ if\ Knock\ Compare > Threshold \quad (2)$$

3. Test methodology

The aim of the test plan is to isolate the effect of ramp duration on transient combustion. A ramp begins with the engine running stably at 2.5 bar IMEP and ends when the engine has reached and held 15 bar IMEP. The ECU adjusts injection pulse width, spark advance and the intake-air setpoint over the commanded ramp duration. All other parameters are held constant — 2,000 rpm, MBT timing (50 % MFB near 8

CAD aTDCf), 30 bar injection pressure, $\lambda = 2.75$, 90 °C coolant and oil, 38 °C intake air. The knock detection uses the calibrated BRIC threshold from Eq. (2); the WOT position that triggers the ramp is mapped into the ECU so that every run begins from the same digital event.

Throughout this study the engine was kept at 2000 rpm to isolate load effects, which can be seen in Table 2. While also maintaining the engine's operation at the Minimum Spark Advance for Best Torque (MBT) which is found to be 50 % MBF of 8 CAD aTDCf up to the maximum spark advance value in the ECU. The injection pressure is kept at 30 bar. The engine is boosted across the set of testing. The knock signal variable (K) represents the intensity of the signal detected by the knock sensor within a specific crank angle period where knock is expected to occur. The reference signal variable (R) represents the background noise which is measured during the crank angle period when knock is not expected to occur. The value of Threshold is a calibrated value that defines the limit of what is considered "normal" combustion. This value is considered the baseline. If the resulting value exceeds the threshold the ECU identifies the event as engine knock based on Equation 2. The setpoint for the firing to be initiated was digitally triggered by opening the throttle to WOT from it being partially opened, this throttle position was mapped into the ECU, to lead to the ECU to react and adjust the engine independent variables accordingly. The DAQ system was constantly running across the log to track how the engine behaved consequently.

Five ramp durations were tested in order from longest to shortest, so that the engine was always approached from a stable baseline before the more severe transients were run. Table 2 lists the ramp set and its qualitative risk class; Table 3 summarises the full test matrix.

The ECU employed in this experiment is a MAHLE Flex ECU, capable of operating in both steady and transient states. It is pre-programmed based on the steady-state conditions for each load step at a fixed lambda, incorporating a lookup table indexed by engine load to command intake boost pressure, fuel injection pulse width, and spark advance. The baseline operating conditions of 2000 rpm and a target lambda of 2.75 were selected based on three primary considerations. Primarily these values leverage an extensive, pre-established steady-state dataset from this experimental setup, which ensures robust accuracy. Additionally, a lambda of 2.75 was chosen to baseline the engine in a stable, lean burn condition. This is ideal when attempting to minimise *NOx* emissions and avoid abnormal combustion such as knock or pre-ignition inherent to hydrogen operation.

These parameters are maintained to ensure each load step is optimised at the Maximum Brake Torque (MBT), corresponding to a CA50 near 8 degrees ATDC. The load is varied by adjusting the throttle valve angular position. The electronic throttle is governed by a PID controller calibrated for critical damping, determined through systematic step-response testing at steady-state. However, in the high-speed transient range (0.24 s–0.48 s), the observed pressure overshoot is not a result of throttle control instability, but rather a pneumatic consequence of manifold-filling dynamics.

The ECU employs a closed-loop control system that uses feedback from a wide-band lambda sensor during transient operations, ensuring that the lambda remains at approximately 2.75. Furthermore, the air intake boost control loop is managed by a PID controller that dynamically responds to fluctuations in lambda during transient ramp durations. This setup ensures precise control for maintaining performance across different load conditions.

Table 2
Test Methodology.

Ramp Time	Classification	Structural Risk
1.38 s	Baseline/Slow	Negligible
1.08 s	Moderate	Low
0.84 s	Moderate	Low
0.48 s	Fast	Moderate
0.24 s	Ultra-Fast/Limit	Critical (Overshoot)

Table 3
Testing Parameters.

Engine Parameters	Unit	Value/Sweep
Engine Speed	RPM	2000
Engine Load (IMEP)	Bar	2.5 → 15
Ramp time	s	1.38, 1.08, 0.84, 0.48, 0.24
Intake Cam	CAD ATDCg	97
Exhaust Cam	CAD BTDCg	102
Start of Injection	CAD BTDCf	150
50 % MBF	CAD ATDCf	8 (up to Rmax Limits)
Injection Pressure	Bar	30
Coolant and Oil Temperature	°C	90
Intake Air Temperature	°C	38
Target Lambda	_	2.75

The dedicated MAHLE ECU, utilising ASCII and purpose-built hardware, can manage internal data flow and logic operations within microsecond ranges. This study highlights the innovative capabilities of the hydrogen transient response in conjunction with a lean combustion process, emphasising the potential for achieving near-zero NOx emissions throughout the entire transient response period. The injection pulse-width modulation (PWM) is regulated by a closed-loop controller that correlates with Indicated Mean Effective Pressure (IMEP) and the output dynamometer torque to ensure load steps are achieved.

Additionally, lambda control is executed in a closed-loop configuration utilising the engine's Mass Air Flow (MAF) sensor, which manages both throttle position and external boost pressure.

4. Results and discussion

The load is set by three ECU outputs: fuel injection pulse width, spark advance and manifold absolute pressure. The figures below track these outputs and the resulting combustion metrics through the five ramps. Two dependencies dominate the discussion: the coupling between boost overshoot and the lambda feedback loop, and how the pressure-gradient metrics (P_{max}, R_{max}) amplify when the loop cannot keep up with the airpath.

4.1. Unburnt hydrogen slip

Before interpreting the transient results, there is a safety limit of 3 % unburnt hydrogen slip which has been established from a previous on this engine which when exceeded the fuel safety cuts the supply. This is another reason to run lean at a lambda of 2.75 as within this region the chance of hydrogen slip to exceed safety limits is improbable. Fig. 1

4.2. Steady-state NOx Benchmark

The steady-state NOx map of this engine at $\lambda = 2.75$ have also been reproduced from our earlier study [21] to anchor the emission argument. NOx formation in hydrogen SI follows the familiar peak: it stays negligible above $\lambda \approx 2.4$ and rises sharply as the mixture is enriched, driven by the adiabatic flame temperature of hydrogen. The $\lambda = 2.75$ target sits about 20 % leaner than the NOx peak, which is a deliberate design margin. Fig. 2 Fig. 4

4.3. Why transient emissions are not measured directly

The transient events considered here last between 240 ms and 1.38 s. Standard chemiluminescent NOx analysers have a T90 response

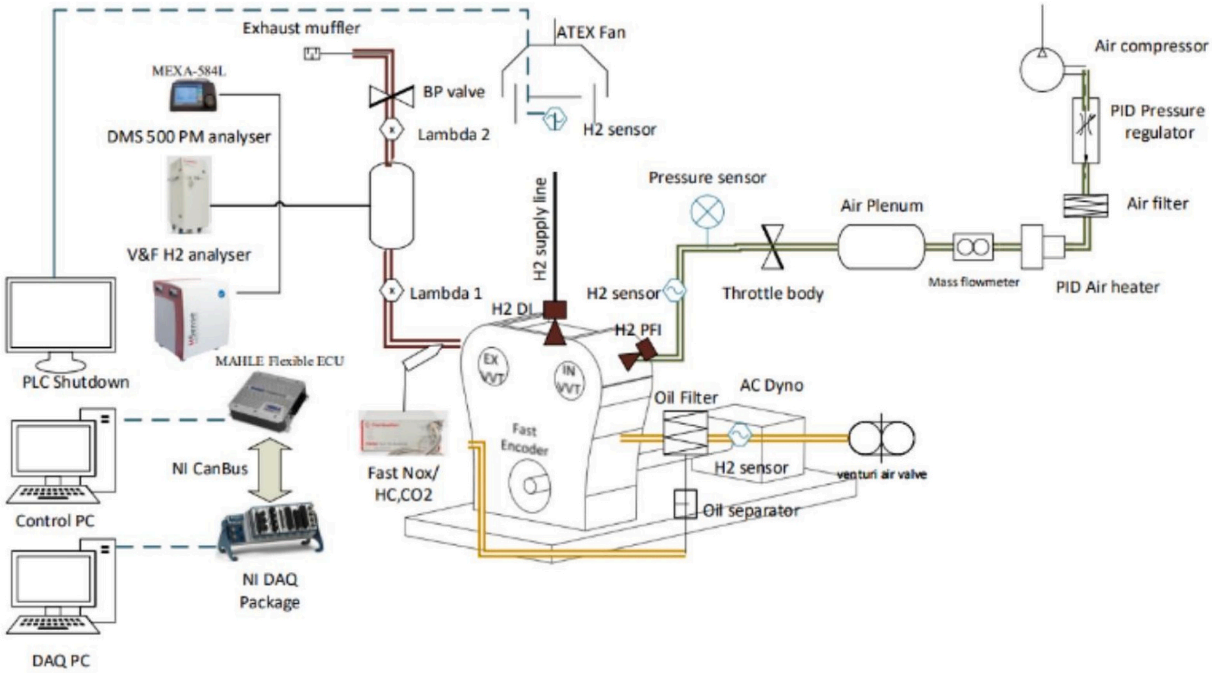

Fig. 1. Test cell schematic.

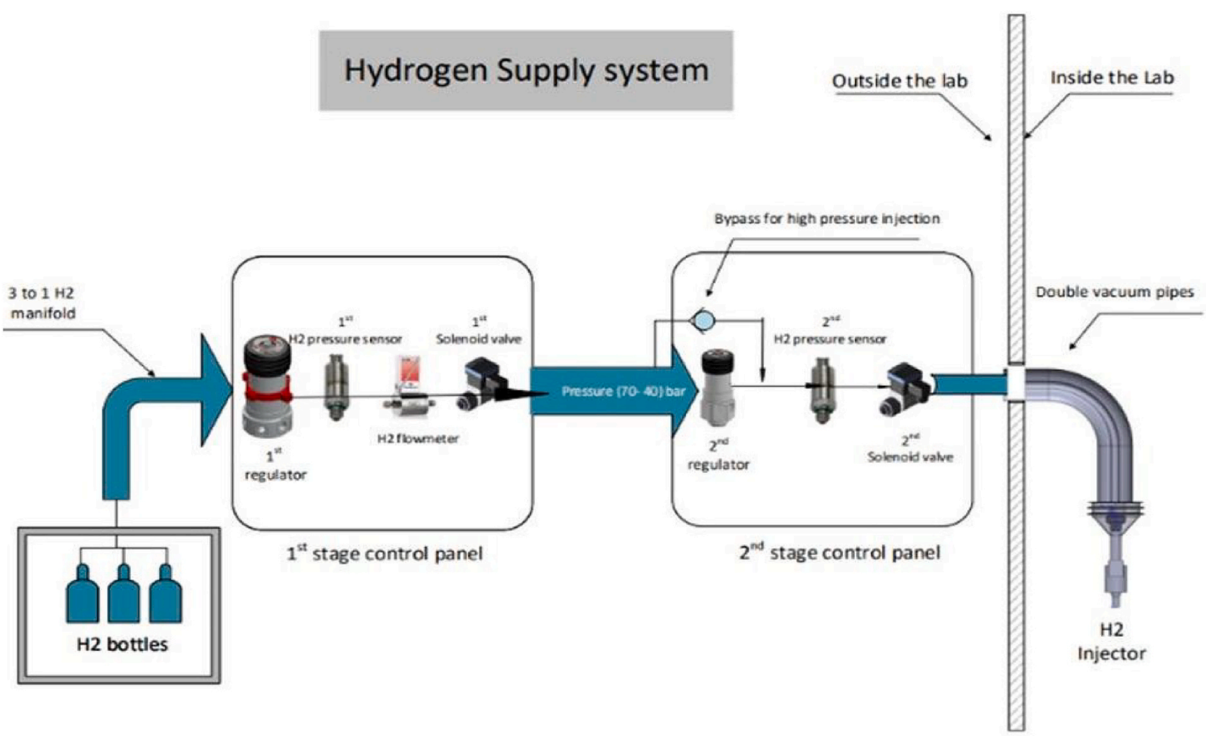

Fig. 2. H2 Supply Line Schematic.

between 1.5 and 3 s once sample-line transport delay is added, and at the high flow speeds seen during rapid load changes the sample is further smeared by mixing inside the probe and line. Together, these effects blur any transient NOx peak well below the cycle-level resolution that would be needed to correlate it with a specific Rmax event. For this reason, NOx emissions are not reported cycle-by-cycle in this paper; the steady-state map of Fig. 5 is used as a proxy sensor, and the λ excursions recorded in Fig. 11 are mapped onto that cliff to infer the emission penalty. A fast CLD is planned for the next campaign and will allow a direct time-domain overlay.

Under steady conditions the load is controlled through in-cylinder thermodynamics and mixture preparation. The injection pulse width sets the injected fuel mass and therefore the energy input. Spark timing positions the heat release relative to TDC, which affects IMEP, stability and thermal efficiency. Intake boost fixes the trapped air mass and thereby the charge density and global λ thereby governing charge density, and the global air–fuel ratio.

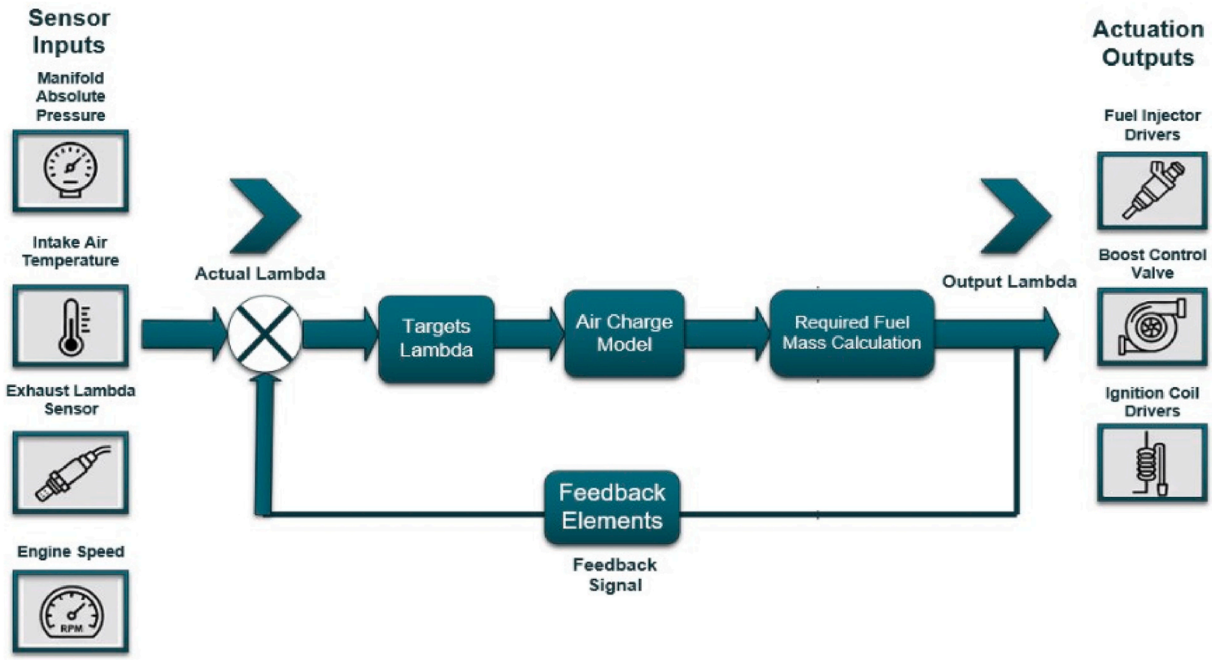

Fig. 3. ECU Closed-Loop Transient.

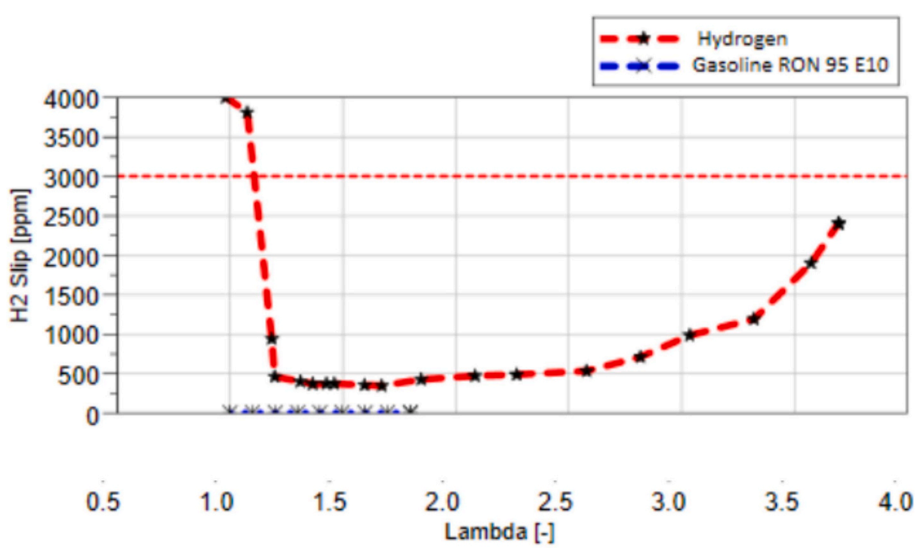

Fig. 4. Steady –state unburnt hydrogen slip (.
reproduced from Mohamed et al. [21])

4.4. Fuel injection pulse width and spark timing

Fig. 6 illustrates the transient response of the injection pulse width (PWM, expressed in milliseconds) and the spark timing (CAD BTDCF) under varying ramp-time configurations. The results demonstrate a strong dependence of system stability and transient behaviour on the selected ramp duration.

At the longest ramp time (1.38 s), the injection response is nonlinear and overdamped. The transition occurs gradually with no observable overshoot, indicating highly damped control. While this strategy promotes stability, it results in prolonged settling times and delayed load realisation.

Below 0.84 s both channels go under-damped: the two shortest ramps show a pronounced overshoot in PWM and a single-step collapse in spark advance; further reduction of ramp time produces significantly faster transient responses accompanied by a pronounced overshoot ratio. The two shortest ramp-time strategies exhibit underdamped behaviour with extreme overshooting. This transient amplification suggests a risk of undesirable combustion and increased cyclic variability.

A comparable trend is observed in the spark timing response. For the 1.38 s ramp, adjustment occurs in two distinct stages: timing initially stabilizes at 13.5° BTDC before a secondary correction to 12.1° BTDC. Steady state is reached after 4 s, reflecting the conservative control strategy of longer ramp durations.

As ramp time decreases, the response becomes increasingly abrupt. Under faster strategies, the adjustment occurs in a single step, transitioning directly from 13.7° → 12.1° BTDC without an intermediate plateau. This significantly shortens the time to steady state but at the expense of transitional smoothness.

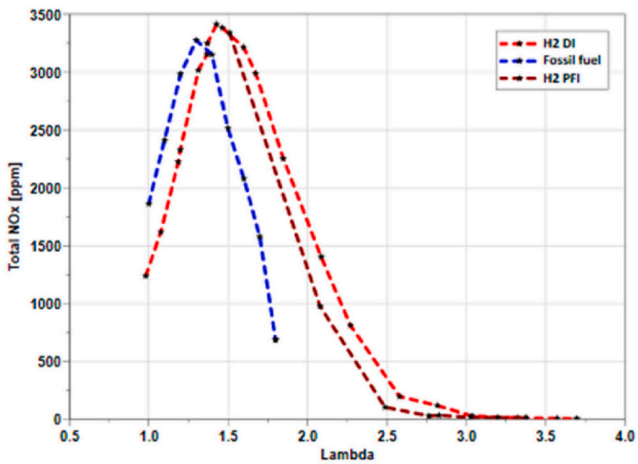

Fig. 5. Steady-state NOx for gasoline and hydrogen over λ (reproduced from Mohamed et al. [21]).

Ramp-time calibration is critical for balancing response speed and dynamic stability. Longer durations promote stable, overdamped behaviour with minimal overshoot, whereas shorter durations enhance responsiveness but introduce underdamped characteristics and transient amplification in both fuel injection and ignition phasing.

4.5. *Boosted intake pressure*

Fig. 7 illustrates Boost response mirrors the PWM response. The 1.38 s case rises slowly and converges smoothly toward the ≈80 kPa target. The 1.08 s case already shows a visible overshoot; at 0.84 s and below the response is aggressive, with a boost spike immediately after the command and a significant deviation from the commanded set-point. The three fastest ramps (0.84, 0.48 and 0.24 s) give similar peak excursions — the system reaches an upper limit in how easily the air path can be forced before the overshoot no longer grows with shorter commanded duration. In physical terms this limitation is a manifold-filling limit rather than a controller-instability limit; the PID is well tuned, but the pneumatic inertia of the intake path is fixed.

Conversely, the 1.08 s ramp displays underdamped characteristics with observable overshoot. As ramp duration is reduced further (0.84 s to 0.24 s), the response becomes increasingly aggressive. A pronounced overshoot occurs immediately following the boost command, with peak pressures approaching 120 kPa substantial deviation from the steady-

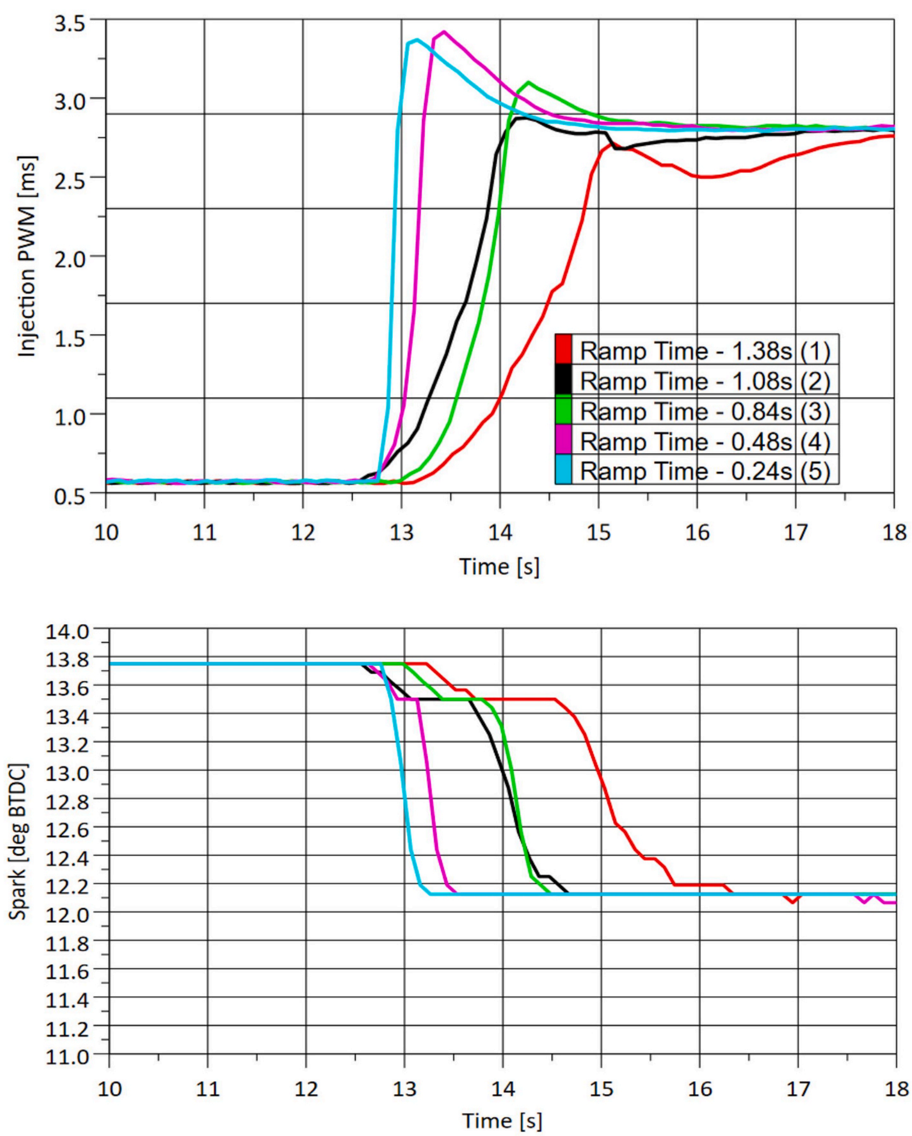

Fig. 6. Injection PWM (ms) and spark timing (CAD bTDCf) vs. time at each ramp duration.

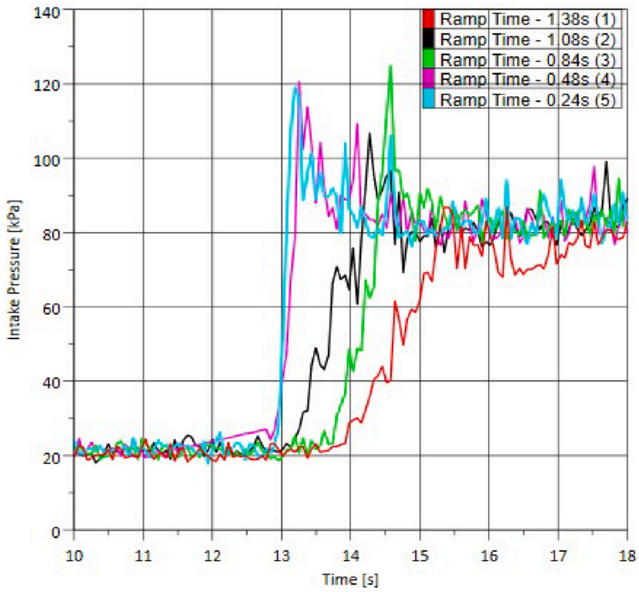

Fig. 7. Boosted intake pressure vs. time at each ramp duration.

state target. Notably, while the overshoot magnitude increases significantly between the 1.08 s and 0.84 s ramps, the peak excursions for the three fastest strategies (0.84–0.24 s) appear to converge. This elevated overshoot ratio indicates insufficient transient damping within the air-path control loop during rapid energy input. The peak transient pressure approaches approximately 120 kPa, representing a substantial deviation from the commanded steady-state target. This elevated overshoot ratio indicates a strongly underdamped system response at shorter ramp durations, characterised by rapid energy input and insufficient transient damping within the air-path control loop.

During the transient load steps, the spark advance was regulated using a rate-limited smoothing function. Although a rapid load ramp (e.g., 0.84 s) theoretically demands a fast-timing shift, a gradual transition was found to be superior for preventing Rmax exceedances. This 'smooth' strategy allows the combustion phasing to transition predictably, providing a buffer against the cycle-to-cycle variability and manifold-filling delays. This approach mitigates the risk of abnormal combustion during the most volatile phase of the torque ramp.

Under the shortest ramps the spark advance is smoothed with a rate limiter. A fast-timing shift is in principle consistent with a fast load ramp, but a gradual spark transition was found to give a more reliable buffer against cycle-to-cycle variability in the torque ramp and protected *Rmax* better than a step. The combustion implications of the boost overshoot are three-fold and motivate the rest of the results section: a transient increase in trapped air mass shifts λ instantaneously away from target before the fuel path can compensate; a sudden rise in charge density can spike peak in-cylinder pressure and torque; and the higher charge density changes the thermodynamic state (burn rate, peak pressure, cyclic variability) in ways the steady-state calibration was not chosen for.

4.6. IMEP

Fig. 8 presents the transient evolution of indicated mean effective pressure (IMEP) at a constant 2,000 rpm. To isolate the effects of ramp-time calibration, all trajectories were synchronised at a T_{10} reference point (10 % load response threshold), ensuring that variations in settling time and overshoot are evaluated from a normalized starting condition. The resulting IMEP response captures the integrated thermodynamic outcome of the coordinated air-path, fuel delivery, and ignition phasing strategies.

For the longest ramp duration (1.38 s), the IMEP trace exhibits an overdamped response. The load increase occurs gradually, with minimal overshoot but an extended settling time before reaching the target load. Although this strategy enhances stability and reduces peak transient stress, it significantly delays torque realisation. As the ramp is shortened the rise time decreases and the overshoot grows monotonically; the 0.48 s and 0.24 s cases peak near 1,800 kPa against a 1,500 kPa target, or about 22 % overshoot. Large IMEP spikes translate directly into impulsive torque on the crank-train and into transient peak in-cylinder pressure, which is the quantity shown next.

Such pronounced load overshoot carries critical combustion and durability implications. Rapid increases in-cylinder pressure elevates peak in-cylinder temperatures and pressure gradients, which may reduce knock margins—particularly under boosted operation. Furthermore, aggressive transient ramping can promote abnormal combustion phenomena, including pressure oscillations and increased cyclic variability (COV_{IMEP}). From a mechanical perspective, these torque spikes impose impulsive stress on the drivetrain and engine components. While shorter ramp times improve responsiveness, the associated overshoot

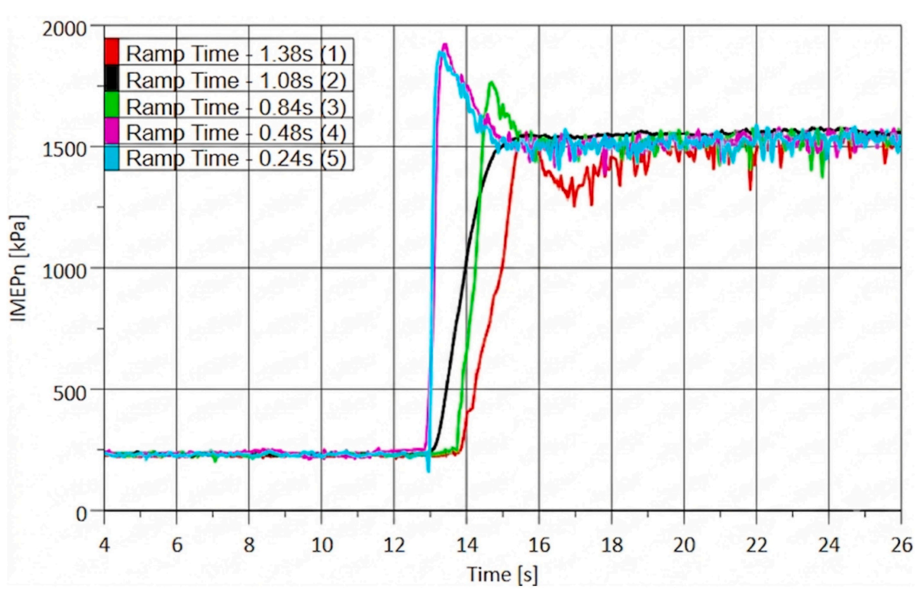

Fig. 8. IMEP vs. time at each ramp duration, aligned on T10 (10 % of load response).

confirms a critical trade-off: excessively aggressive calibration may compromise both knock control and transient lambda stability.

4.7. Peak in-cylinder pressure

As illustrated in Fig. 9 the two fastest ramps drive P_{max} to surpass the 120-bar mechanical design limit of the engine (steady state operation limit) — a margin of only a few bar in some cycles. It is critical to distinguish between the engine's operational limits under different combustion regimes: the continuous mechanical fatigue threshold is restricted to 120 bar under steady-state operating conditions, whereas the hardware is structurally rated to withstand peak instantaneous pressures of up to 160 bar during transient variations and abnormal combustion events (such as high-intensity knocking or pre-ignition).

The 0.24 s case achieves its steady-state pressure faster than 0.48 s, but the approach is under-damped, and the intermediate peak is the problem, not the final value. The 1.38 s case is heavily damped: the rise is slow, low-amplitude oscillations persist before the trace settles, and at no point does P_{max} come close to the design limit. Of the five ramps the 1.08 s case is arguably the best dynamic compromise — the overshoot is small, stabilisation is faster than at 1.38 s, and P_{max} never gets within a meaningful margin of the structural ceiling.

In contrast, the 1.38 s ramp produces a heavily damped pressure rise with significantly reduced overshoot. While this conservative strategy protects against extreme pressure excursions, the settling process is extended, and low-amplitude fluctuations persist longer before reaching steady state. This results in a superior safety margin at the expense of delayed torque realization. Overall, these results confirm that (P_{max}) transients are the primary limiting factor in aggressive ramp-time calibration, necessitating a balance between load-tracking speed and structural integrity.

The 1.08 s intermediate ramp duration offers a superior dynamic compromise. While a modest overshoot is present, its magnitude remains significantly below that of the 0.48 s and 0.24 s strategies. Aggressive calibration amplifies transient intake pressure overshoot, which directly translates into peak combustion pressures approaching the 160-bar mechanical design limit. Conversely, excessively slow ramping attenuates pressure excursions but prolongs load response latency. These findings demonstrate a strong coupling between air-path control and combustion intensity during load transients.

4.8. Maximum Pressure-rise rate

Fig. 10 illustrates the transient evolution of the maximum pressure rise rate (R_{max}); a structural safety threshold of 600 kPa/°CA is imposed to prevent excessive combustion induced stress, with nominal steady-state values stabilizing near 300 kPa/°CA. The results reveal a high sensitivity of R_{max} to the selected ramp-time calibration. The 1.38 s strategy is the only configuration that successfully completes the load transition without violating the 600 kPa/°CA safety limit. While this slower response increases latency, the combustion pressure development remains effectively damped, preventing the transient heat-release amplification observed in more aggressive strategies. This suggests that a ramp duration of 1.38 s provides the necessary buffer to maintain combustion harshness within calibrated reliability envelopes during rapid load steps.

In contrast, all ramp strategies shorter than 1.38 s exceed the 600 kPa/°CA safety limit during the transient phase. The 0.48 s ramp exhibits the most severe amplification, with (R_{max}) peaking near 1,000 kPa/°CA—over three times the steady-state target. Interestingly, the fastest ramp (0.24 s) produces a slightly lower peak of approximately 800 kPa/°CA, comparable to the intermediate 0.84– 1.08 s cases, yet still well above calibrated thresholds.

R_{max} is the single most sensitive combustion-severity metric in this sweep. The engine here has a steady-state working point near 300 kPa/°CA; of the five ramps only the 1.38 s case stays below 600 kPa/°CA throughout the whole log. The 0.48 s case is the worst, peaking near 1,000 kPa/°CA — more than three times the steady-state target and roughly 1.7 times the structural limit. The 0.24 s case peaks near 800 kPa/°CA: shorter duration is not always worse, as the fuel and air paths become more tightly coupled in time at the very shortest ramp, whereas at 0.48 s the two paths are separated by just enough delay to amplify the transient. The 0.84 s and 1.08 s cases sit between these, but both still violate the calibrated threshold. The mechanism is a direct coupling of boost overshoot to the lambda feedback loop: the abrupt increase in trapped air mass runs ahead of the fuel-path response, heat release rates accelerate, and the pressure gradient follows. From a durability standpoint the 0.48 s case is the most damaging — not because the single peak is highest, but because the amplification is sustained over several cycles and so imposes repeated impulsive loading on the piston, rings and bearings rather than a single high-amplitude excursion.

4.9. Excess-air ratio (λ) trajectory

Fig. 11 gives the mechanism behind the R_{max} results. At the load step λ spikes lean (≈ 3.2 in the fastest cases) As trapped air grows faster than the fuel path can compensate. The closed-loop lambda controller then over-fuels to correct the lean spike, and λ dips to roughly 2.1–2.2 before settling at 2.75. This lean-to-rich oscillation is the transient lambda excursion that the rest of the paper attributes R_{max} to the abrupt

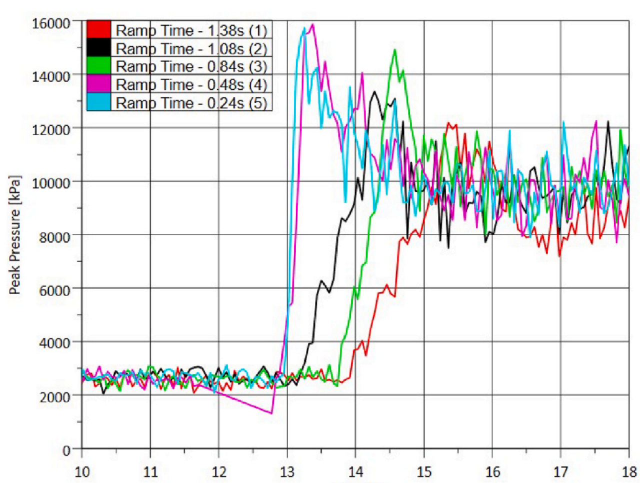

Fig. 9. Peak in-cylinder pressure (Pmax) vs. time at each ramp duration.

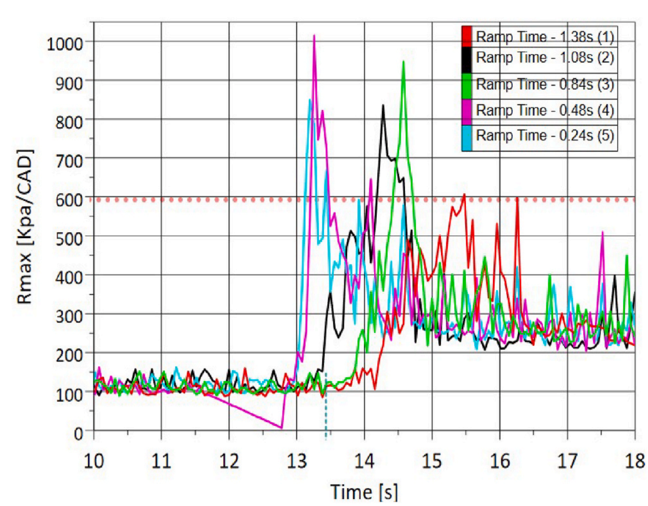

Fig. 10. Maximum Pressure Rise Rate (Rmax) vs. Time at each Ramp Duration.

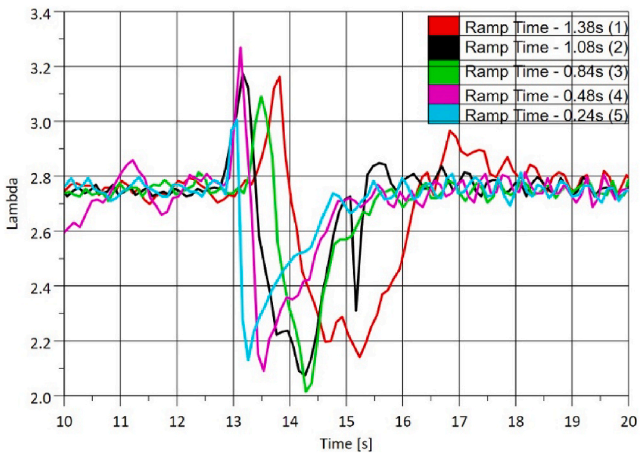

Fig. 11. Excess-air ratio (λ) vs. time at each ramp duration; target λ = 2.75.

enrichment accelerates heat release and lifts dP/dθ. The 0.48 s case shows the deepest enrichment dip, which is consistent with its appearance as the R_{max} peak in Fig. 10 — the simultaneous presence of excess trapped air and excess fuel briefly shifts mixture reactivity into a very intense combustion regime. The 1.38 s case shows the same qualitative shape but with much smaller amplitude; λ never overshoots far enough to push R_{max} past its threshold.

Subsequently, the closed-loop lambda controller compensates by increasing the injected fuel mass, inducing a rapid enrichment phase. λ drops to approximately 2.1–2.2 before stabilizing at the nominal 2.75 target upon conclusion of the ramp event. This abrupt transition from lean (λ ≈ 3.2) to rich (λ ≈ 2.1) conditions represents a substantial transient air–fuel ratio oscillation.

A direct correlation exists between λ excursions and R_{max} amplification. The pressure rise rate is highly sensitive to the air–fuel ratio under boosted hydrogen operation; specifically, the rapid enrichment following an initial lean spike accelerates the heat release rate, increasing the pressure gradient ($dP/d\theta$). This overshoot– undershoot cycle provides the mechanistic explanation for the R_{max} spikes recorded in Fig. 8.

As evidenced by the injection PWM response (Fig. 3), fuel overshot during low λ phases compounds this effect; the simultaneous presence of excess trapped air and excess fuel abruptly shifts mixture reactivity. Conversely, the 1.38 s ramp exhibits moderated λ transitions with reduced enrichment depth. Although minor oscillations persist and delay steady-state stabilization, the reduced amplitude of the λ deviation ensures that R_{max} remains within calibrated reliability limits. These results confirm that transient combustion severity is governed by the coupled dynamics of boost control and lambda regulation.

4.10. A feed-forward correction for lambda during fast ramps

The change in lambda during the transient shifts the combustion duration much more drastically than it would in a gasoline engine, the determining factor being the laminar flame speed being significantly higher than gasoline while also being more sensitive to λ.

1 The Theoretical Framework (The Prediction)

To address the observed λ excursions during rapid load transitions, as the enrichment dip is driven by the controller reacting after the air-path has already moved, a purely reactive lambda loop cannot close the gap at the shortest ramps. The obvious countermove is to add a feed-forward fuelling term keyed off the measured rate of intake-pressure change, so that fuel mass begins to change before the lambda sensor sees the lean spike. Steady-state mapping on this engine gives a linear correlation between intake manifold pressure and the fuel mass required to maintain the λ target, from which a Fuel Sensitivity Factor can be defined:

$$\mathrm{Kff} = \frac{\Delta mf\ \mathrm{steady}}{\Delta P_{intake}} \tag{3}$$

At the 0.24 s ramp the air path has essentially completed its filling step before the closed-loop fuel correction has settled. IMEP overshoots the target by about 22 % and the lambda trace shows the deep enrichment dip discussed above. A steady-state comparison of the fuel mass delivered during the ramp against the mass predicted from $K_{ff} \cdot \Delta P_{intake}$ indicates that the engine is running fuel-deficient during the first portion of the fastest ramps, which is why the lean spike is so pronounced.

2 Quantifying the control gap

Analysis of the 0.24 s transient ramp reveals a significant "Control Gap" between the current feedback-only ECU logic and the physics-based requirements. While the P_{intake} rose rapidly, the results show that the ignition phasing and injection settling time require approximately 4 ss to reach a stable steady-state. In the 0.24 s ramp, this creates a massive delay where the air-path overshoots almost immediately, but the closed-loop stabilization lags by several seconds.

Furthermore, the recorded IMEP peak of 1,800 kPa against a target of 1,500 kPa indicates a 22 % transient load error. By comparing these transient fuel delivery values to the steady-state, it is determined that the current system operates with a critical fuel deficit during the initial phase of the ramp, directly leading to the observed NOx-prone rich spikes.

3 The Hydrogen-Specific transient correction factor

As hydrogen has no wall-wetting reservoir and mixing is dominated by the instantaneous pressure ratio, the feed-forward gain needed at fast ramps is larger than the steady-state K_{ff} would predict. A hydrogen-specific correction term scaled by dP/dt captures this:

$$m_{f,corrected} = m_{f,feedback} + (\sigma_{H2}.dP/dt \tag{4}$$

Maintaining λ > 2.5 is critical for near-zero NOx operation. The transient excursions to λ = 2.1 observed in the 0.24 s ramp suggest a significant NOx penalty that requires this higher feed-forward gain to "pre-actuate" injectors before the air path manifold filling is complete. This approach shifts the control focus from reactive correction to proactive physics-based estimation, providing a robust pathway for zero-emission H2 combustion during real-world dynamic operation.

This is a proposal, not a validated controller. Eqs. (3), (4) provide a principled way to shift the lambda loop from reactive correction toward physics-based pre-actuation, but tuning σ_H2 and quantifying its benefit on Rmax require a closed-loop test that is out of scope here and is listed as future work in Section 5. The point of raising it now is that the experimental data identify exactly which control gap a feed-forward term would need to fill.

4.11. Burn duration (CA10-CA90)

Fig. 12 illustrates that although boost, IMEP, Pmax, Rmax and λ all swing strongly through the transient, the 10–90 % burn duration does not. Once λ settles close to 2.75 the CA10–CA90 interval converges to a consistent value across every ramp. Transient deviations in burn duration during the immediate load step are comparatively small relative to the pronounced excursions observed in R_{max} and P_{max}. The 1.38 s case is slightly smoother during the transient itself, and the faster ramps show small short-lived fluctuations that decay quickly. The practical implication is important: transient calibration on this architecture does not need to manage burn duration, it needs to manage the pressure gradient.

Once the target excess air ratio (λ ≈ 2.75) is restored and engine speed then remains fixed, the CA10–CA90 interval converges to a consistent value, indicating robust combustion control under steady-state lean operation. Among the ramp strategies, the longest ramp duration (1.38 s) exhibits slightly smoother burn duration evolution during the transient phase, with reduced short-term fluctuation compared to the faster ramps. In contrast, shorter ramp times show

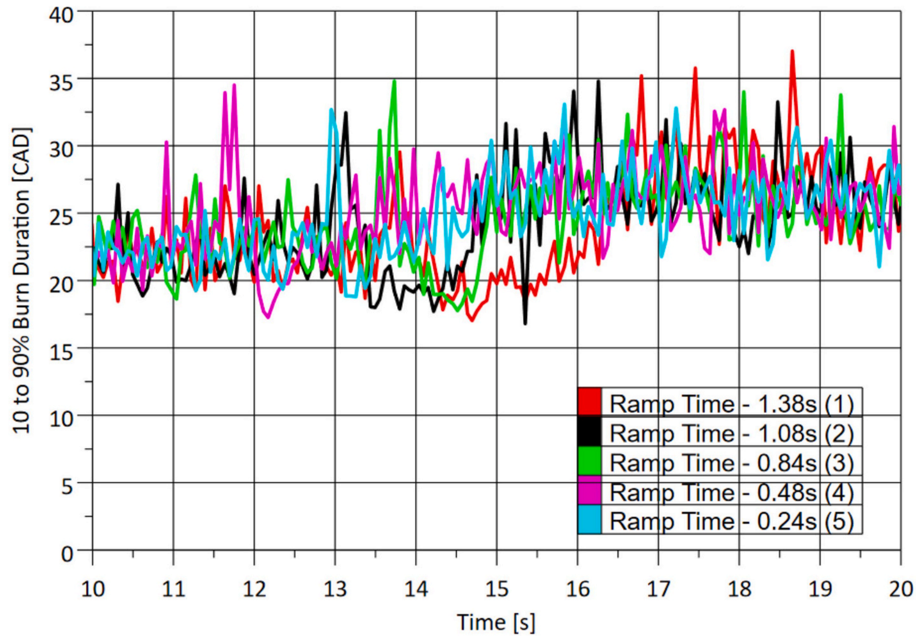

Fig. 12. 10–90 % burn duration [CAD] vs. time at each ramp duration.

marginally increased oscillatory behaviour during the initial load transition; however, these deviations remain limited and rapidly converge to steady-state values.

The similarity in burn duration between low-load and high-load steady-state conditions indicates that combustion efficiency and heat release development remain well-controlled once transient disturbances subsides. Consequently, the primary constraint for transient calibration in this architecture is the management of peak pressure rise rates rather than the stabilization of the overall combustion phasing.

The steady-state baseline calibration, set a spark advance targeting a CA50 of 8° CA ATDC which was established as the optimal MBT timing based on years of data previously conducted using this exact engine. However, as evaluated across the rapid transient load sweeps, CA50 did not remain perfectly constant at this target. Due to the inherent response lag between the rapid fuel injection adjustments and the air intake track dynamics, significant instantaneous variations in the lambda (Fig. 11) and in-cylinder turbulence intensity occurred during the fast transitions. As the open-loop spark timing control was mapped strictly to instantaneous engine speed and intake manifold pressure targets without active closed-loop cylinder-pressure feedback or dynamic transient spark advance compensation, these slight variations in CA50 directly reflect the raw thermodynamic and chemical kinetic response of the mixture under uncompensated transient conditions.

Regarding the specific transient execution method of the Maximum Brake Torque (MBT) strategy, the engine control unit (ECU) utilized a pre-mapped, open-loop feedforward control architecture. Under steady-state operating conditions, the baseline spark advance MBT required to maintain the optimal combustion phasing of CA50 $= 8^{\circ}$ CA ATDC was mapped comprehensively as a function of engine speed and intake manifold pressure P_{intake}. During the execution of the rapid transient load ramps 1.38 s down to 0.24 s, the ECU dynamically tracked the instantaneous change in intake manifold pressure to look up the corresponding spark advance target. However, as the transient execution relied strictly on these static steady-state lookup tables, it lacked an active, closed-loop cylinder-pressure feedback loop or a dedicated dynamic transient spark advance correction algorithm. Consequently, the control system was unable to compensate on the fly for the ignition delay shifts caused by instantaneous relative air–fuel ratio lambda oscillations or changing in-cylinder residual gas fractions during the fast mass flow transitions.

Interestingly, despite these localized CA50 deviations and the drastic instantaneous fluctuations in both lambda and pressure rise rates, the overall CA10-CA90 main combustion duration remains remarkably stable and highly synchronized across all test cases, as illustrated in Fig. 12 Regardless of whether the load is ramped gently over 1.38 s or accelerated aggressively in 0.24 s, the burn duration profiles sit tightly within the same localized band.

This stability is governed by a self-compensating thermodynamic balancing act inherent to hydrogen lean-burn operation, where two opposing physical phenomena compete during a rapid load increase:

The Chemical Kinetic Effect: Momentary lean spikes or air–fuel tracking delays tend to decrease the local laminar burning velocity of the hydrogen mixture, which acts to prolong the combustion duration.
The Thermal and Aerodynamic Effect: Concurrently, the rapid increase in intake manifold pressure elevates the unburned gas density, substantially boosting the in-cylinder turbulent kinetic energy and compression temperature prior to ignition. Because the laminar burning velocity of hydrogen scales exponentially with unburned gas temperature this thermal and aerodynamic enhancement significantly accelerates flame propagation.

As both competing drivers scale proportionally with the absolute change in intake mass flow, they effectively counterbalance each other regardless of the transient acceleration rate. This explains why the five distinct ramp traces overlap so cleanly. Furthermore, the global upward shift in the average burn duration observed across all cases moving from approximately 22° CA at 10 s to 27° CA at 20 s reflects the macro-level transition of the engine operating point as the load stabilizes at its new target, completely independent of the dynamic ramp speed itself.

4.12. Knock intensity

Fig. 13 illustrates the BRIC-based knock trace (Eq. 2) through each ramp shows three distinct regimes. At 0.24 s a single high amplitude knock spike appears immediately after the load step, driven by the combined effect of boost overshoot, elevated Pmax and rapid combustion phasing. After that single event the intensity returns below threshold. At 0.48 s the system shows multiple threshold violations through the transient, several knock events rather than one, which from

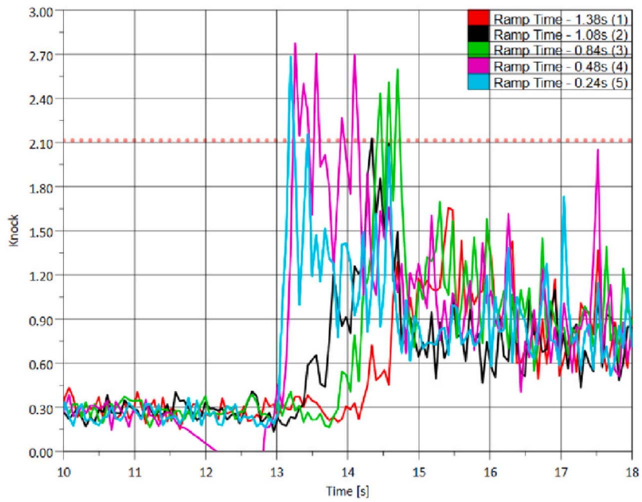

Fig. 13. Knock intensity [-] against time at different ramp time.

a fatigue standpoint is more damaging than the single high-amplitude spike at 0.24 s. At 0.84 s the onset of knock activity is delayed but the transient carries roughly three above-threshold events before stabilising, with one late excursion approaching 150 bar peak pressure that indicates controller saturation on the air path: the fuel mass increases abruptly that allows λ to drift further than the lambda loop can pull back. The 1.38 s case stays below the knock threshold for the whole transient.

These findings confirm that aggressive air-path and load actuation drive the combustion system into a knock-limited regime. While faster ramps reduce response latency, they concurrently decrease the knock margin, necessitating retarded ignition phasing or enriched mixtures to maintain structural integrity. Conversely, the 1.38 s strategy provides sufficient damping to ensure knock-free operation throughout the load transition. Distinct knock characteristics are observed among the faster ramp strategies:

0.24. S ramp(fastest)

A single pronounced knock spike occurs immediately following the load increase. After this initial excursion, the system stabilises rapidly and knock intensity returns to sub-threshold levels. Although limited to a single primary event, the spike's amplitude is significant due to the combined effects of boost overshoot, elevated peak pressure, and rapid combustion phasing.

0.48. S ramp

This configuration exhibits multiple knock events during the transient phase. The repeated excursions above the knock threshold indicate sustained combustion instability rather than a single amplified event. From a durability perspective, repeated knock cycles are potentially more detrimental than a single high-amplitude spike, as cyclic structural loading may accelerate fatigue damage.

0.84. S ramp

A delayed knock response is observed, characterised by approximately three transient spikes above the threshold before stabilisation. This suggests that intermediate ramp speeds may induce a prolonged period of mixture and pressure oscillation before steady-state combustion is achieved.

The knock trends correlate strongly with previously observed transient dynamics in boost pressure, peak in-cylinder pressure, R_{max}, and lambda fluctuation. Rapid boost ramping increases trapped charge density, while injection PWM overshoot and aggressive lambda correction amplify heat release rate. These combined effects intensify end-gas conditions, thereby increasing knock propensity. Interestingly, the fastest ramp (0.24 s) produces a single but sharp knock event, whereas the 0.48 s ramp results in multiple knock occurrences. This highlights an important calibration insight: reducing ramp duration does not guarantee reduced knock severity. Instead, knock behaviour depends on the interactions among boost dynamics, fuel response, ignition phasing, and the lambda correction strategy. The 0.84 s ramp demonstrates a slightly delayed start followed by a much more aggressive and uncontrolled pressure rise, peaking at near 15,000 kPa. At 0.84 s, the fuel mass is increasing so rapidly that the resultant lambda deviates too far from the target. The controller then overcompensates, leading to the higher peak pressures and sustained oscillations seen between 14.5 s and 16 s.

Knock analysis using the BRIC method confirms that aggressive ramping increases the probability of abnormal combustion, manifested as single or multiple knock events during the transition. Conversely, the 1.38 s ramp yields a well-damped response that maintains R_{max} within safe limits and minimises knock activity, albeit at the cost of torque realisation. Notably, burn duration (CA10–CA90) remains invariant across all strategies once steady-state is achieved. This indicates that transient combustion severity is governed by pressure gradient amplification ($dP/d\theta$) rather than fundamental destabilisation of the total burn duration. These findings underscore a critical trade off: optimised ramp calibration must balance response speed against the necessity for controlled boost, λ stability, and R_{max} limitation to ensure the durability of downsized, boosted architectures.

4.13. Cause-effect chain

Reading the figures together gives a consistent deterministic chain. An intake-pressure overshoot forces a compensating injection PWM overshoot as the ECU corrects the lean shift caused by the air surge; that correction produces the lambda dip; the lambda dip accelerates heat release; heat-release acceleration produces the Pmax and Rmax transients; and the pressure-gradient transient drives the knock events observed at faster ramps. Under 2,000 rpm operation, the feedback loop can keep this chain bounded only for ramps around 1.38 s. For any shorter ramp the pneumatic response of the intake outruns the lambda-loop bandwidth, and the system leaves the calibrated safe envelope.

5. Conclusions

A systematic analysis of the transient ramp-duration sweep (ranging from 1.38 s to 0.24 s) reveals four primary thermodynamic and mechanical conclusions. First, the transient ramp duration acts as a first-order calibration variable: shortening the transition timeline sharpens the immediate load response but severely amplifies transient overshoots in intake manifold pressure, net indicated mean effective pressure (IMEPn, peak in-cylinder pressure P_{max}), and the maximum pressure rise rate (R_{max}). Second, the pressure gradient (R_{max}) constitutes the definitive binding calibration constraint. Only the 1.38 s baseline ramp successfully maintained combustion harshness within the 600 kPa/°CA structural reliability threshold across the entire transition. Conversely, the 0.48 s strategy induced the most severe operational boundary violation, peaking at approximately 1,000 kPa/°CA, while the ultra-fast 0.24 s ramp generated a slightly lower, yet still unacceptable peak near 800 kPa/°CA. Third, the underlying governing mechanism is consistent across all evaluation metrics, driven by the dynamic lambda lean-to-rich tracking oscillation mechanism detailed thoroughly in Section 4.8. Fourth, once the relative air–fuel ratio stabilizes, the main combustion duration (CA10-90 %) remains essentially invariant with respect to the transient execution rate. This confirms that transient severity on this direct-injection platform is fundamentally a pressure-gradient constraint rather than a macro-burn rate limitation.

From a calibration perspective, only the conservative 1.38 s ramp duration can be classified as unambiguously safe under the current engine configuration. The 1.08 s trajectory represents a marginal boundary point: while P_{max} and IMEPn characteristics remain within acceptable structural fatigue limits, R_{max} systematically violates the 600 kPa/°CA reliability threshold. Consequently, it cannot be recommended as a safe operational boundary under a conventional feedback-only control strategy. Executing any transient load step faster than 1.38 s at an operating baseline of lambda = 2.75 mandates either an altered transient combustion calibration—such as localized ignition timing retardation or strategic lambda enrichment restricted strictly to the dynamic window—or the implementation of a feed-forward fuelling compensation term scaled by the rate of intake manifold pressure change (dP/dt), predictive control action is required to proactively suppress the transient air–fuel tracking gap before it manifests as a destructive pressure-gradient anomaly.

The operational limitations of the present study must be contextualized, the current experimental campaign deliberately focused on a single engine speed baseline (2000 rpm) and a fixed direct-injection strategy. This boundary was strategically selected to leverage an extensive, pre-validated steady-state database that established this specific operational window as highly robust against abnormal combustion. Given that ultra-fast load transitions introduce severe risks of catastrophic pre-ignition, backfire, and extreme rates of pressure rise, isolating the transient acceleration rate within a known safe thermal and kinetic region was imperative to ensure hardware security. While this tightly controlled single-condition limitation allowed for the precise isolation of the fundamental transient self-compensation mechanisms of the hydrogen flame front, it inherently limits immediate extrapolation to multi-dimensional vehicle operating maps. Consequently, safely expanding this transient analysis to multi-speed operating blocks and adaptive injection timing strategies constitutes the next logical phase of this research.

Three pieces of work follow from this study and are already planned. A fast CLD will be added to the exhaust line so that the transient NOx penalty inferred here from the steady-state cliff can be measured directly. The feed-forward controller described in Section 4.9 will be implemented on the MAHLE FlexECU and validated against the present ramp sweep. Finally, the lambda-loop parameters identified here will be used as the baseline for the per-cylinder fuelling logic in a multi-cylinder turbocharged version of the platform, where wastegate dynamics and manifold resonance will be added to the same control architecture.

CRediT authorship contribution statement

Zayne Zaman: Writing – review & editing, Writing – original draft, Investigation, Formal analysis, Data curation. **Mohamed Mohamed:** Writing – review & editing, Writing – original draft, Formal analysis. **Xinyan Wang:** Writing – review & editing, Supervision. **Hua Zhao:** Writing – review & editing, Writing – original draft, Supervision, Methodology. **Anthony Harrington:** Resources, Methodology, Investigation. **Jonathan Hall:** Project administration, Resources.

Declaration of competing interest

UKRI has funded this research, and MAHLE Powertrain provides the experimental power unit. Clean Air Power and Phinia provide the Hydrogen DI and PFI injectors.

Data availability

Data will be made available on request.

References

[1] Fulton LM, Lynd LR, Körner A, Greene N, Tonachel LR. The need for biofuels as part of a low carbon energy future. Biofuels Bioprod Biorefin 2015;9(5):476–83. https://doi.org/10.1002/bbb.1559.

[2] Florini A. The international energy agency in global energy governance. Glob Policy 2011;2(1):40–50. https://doi.org/10.1111/j.1758-5899.2011.00120.x.

[3] Schlacke S, Wentzien H, Thierjung EM, Köster M. Implementing the EU climate law via the 'Fit for 55' package. Oxford Open Energy 2022;1:oiab002. https://doi.org/10.1093/ooenergy/oiab002.

[4] Verhelst S, Wallner T., Hydrogen-fueled internal combustion engines. Prog Energy Combust Sci 2009;35(6):490–527. 10.1016/j.pecs.2009.08.001 *(Note: Combined duplicate entries from original and [9])*.

[5] Turns SR, Haworth DC. An introduction to combustion: Concepts and applications. 4th ed. New York, NY: McGraw-Hill Education; 2021.

[6] Staffell I, Scamman D, Abad AV, Balcombe P, Dodds PE, Ekins P, et al. The role of hydrogen and fuel cells in the global energy system. Energy Environ Sci 2019;12 (2):463–91. https://doi.org/10.1039/c8ee01157e.

[7] Wang X, Sun B, Luo Q. Transient performance and control strategy of a turbocharged hydrogen internal combustion engine. Int J Hydrogen Energy 2019; 44(26):13983–93. https://doi.org/10.1016/j.ijhydene.2019.03.264.

[8] Christoforetti P, Kappacher P, Schutting E, et al. Experimental investigation into transient operating strategies of a turbocharged lean-burn hydrogen ICE and comparison to diesel performance. Automot Engine Technol 2025;10:13. https://doi.org/10.1007/s41104-025-00159-5.

[9] Aston Martins, Hybrid Hydrogen Rapide S: Technical specifications and development. AstonMartins.com; 2013 [updated 2024; cited 2026 Feb 26]. Available from: https://astonmartins.com/car/hybrid-hydrogen-rapide-s/.

[10] Mohamed M, Longo K, Zhao H, Hall J, Harrington A. Hydrogen engine insights: a comprehensive experimental examination of port fuel injection and direct injection. SAE Technical Paper 2024. https://doi.org/10.4271/2024-01-2611.

[11] Mohamed M, Biswal A, Wang X, Zhao H, Hall J. Experimental investigation for enhancing the performance of hydrogen direct injection compared to gasoline in spark ignition engine through valve timings and overlap optimization. Fuel 2024; 372:132257. https://doi.org/10.1016/j.fuel.2024.132257.

[12] Mohamed M, Feng Y, Wang X, Zhao H, Hall J. Investigating the impact of compression ratio on hydrogen combustion and emission: an experimental analysis. Int J Engine Res 2024. https://doi.org/10.1177/14680874251341641.

[13] Mohamed M, Mirshahi M, Jiang C, Zhao H, Harrington A, Hall J. Hydrogen injection position impact: experimental analysis of central direct injection and side direct injection in engines. SAE Int J Engines 2024;17(5):38–51. https://doi.org/10.4271/03-17-05-0038.

[14] Mohamed M, Biswal A, Wang X, Zhao H, Harrington A, Hall J. Unveiling the potential of hydrogen in a downsized gasoline direct injection engine performance and emissions experimental study. SAE Int J Fuels Lubr 2024;17(3):15–28. https://doi.org/10.4271/04-17-03-0015.

[15] Mohamed M, Biswal A, Wang X, Zhao H, Harrington A, Hall J, et al. Exploring the benefits of hydrogen-water injection technology in internal combustion engines: a rigorous experimental study. Int J Engine Res 2024. https://doi.org/10.1177/14680874241288624.

[16] Babayev R, Im HG, Andersson A, Johansson B. Hydrogen double compression-expansion engine (H2DCEE): a sustainable internal combustion engine with 60%+ brake thermal efficiency potential at 45 bar BMEP. Energy Convers Manag 2022; 264:115698. https://doi.org/10.1016/j.enconman.2022.115698.

[17] Li H, Karim GA. Knock in spark ignition hydrogen engines. Int J Hydrogen Energy 2004;29(8):859–65. https://doi.org/10.1016/j.ijhydene.2003.09.013.

[18] Heinold A. Control and Combustion Stability of Hydrogen Internal Combustion Engines during Load Transients [Dissertation]. 2024.

[19] Heinold A, et al. Research on transient performance of PFI hydrogen internal combustion engine. SAE Technical Paper 2025–01-7110; 2025.. https://doi.org/10.4271/2025-01-7110.

[20] Guzzella L, Onder CH. Introduction to modeling and control of internal combustion engine systems. 2nd ed. Berlin Heidelberg: Springer-Verlag; 2010. 10.1007/978-3-642-10775-7.

[21] Mohamed M, Wang X, Zhao H, Peckham M, Hall J, Jiang C. A Comprehensive Experimental investigation of NOx emission characteristics in hydrogen engine using an ultra-fast crank domain measurement. Energies 2024;17(16):4141. https://doi.org/10.3390/en17164141.